Research Article | Vol. 29, No. 8 / 12 April 2021 / Optics Express 12033
Optics EXPRESS

Room-temperature Fe:ZnSe laser tunable in the spectral range of 3.7–5.3 µm applied for intracavity absorption spectroscopy of CO_2 isotopes, CO and N_2O

PETER FJODOROW,[1,*] MIKHAIL P. FROLOV,[2] YURI V. KOROSTELIN,[2] VLADIMIR I. KOZLOVSKY,[2] CHRISTOF SCHULZ,[1] STANISLAV O. LEONOV,[2,3] AND YAN K. SKASYRSKY[2]

[1]*Institute for Combustion and Gas Dynamics – Reactive Fluids, University of Duisburg-Essen, Lotharstr. 1, 47057 Duisburg, Germany*
[2]*P.N. Lebedev Physical Institute of the Russian Academy of Sciences, Leninskiy Prosp. 53, 119991 Moscow, Russia*
[3]*Bauman Moscow State Technical University, 2nd Baumanskaya str. 5, 105005 Moscow, Russia*
[*]*peter.fjodorow@uni-due.de*

Abstract: We demonstrate an intracavity absorption spectroscopy system based on a broadband single-crystal pulsed Fe:ZnSe laser. The laser operates at room-temperature and is continuously tunable in the spectral range of 3.76–5.29 µm. The long-wavelength emission up to 5.29 µm is a record achievement for Fe:ZnSe lasers, to the best of our knowledge. The developed laser system is applied for measurements of gaseous absorption inside the laser resonator. We demonstrate sensitive detection of (i) CO_2 isotopes in the atmosphere and in human breath, (ii) CO in breath (after cigarette smoking) and in the smoke of a smoldering paper, and (iii) N_2O in a gas flow. The achieved detection limits are: 0.1 ppm for $^{12}CO_2$ and $^{13}CO_2$, 3 ppm for CO, and 1 ppm for N_2O. The sensitivity of the current system is primarily limited by the short pump-pulse duration of 40 ns. Possibilities for sensitivity enhancement by up to a factor of 10^7 are discussed.

1. Introduction

The mid-infrared (MIR) spectral range currently attracts a growing attention due its high potential for numerous applications. As a result, a rapid progression in technologies associated with generation and detection of MIR radiation can be observed. One of the fields particularly benefiting from these developments is laser spectroscopy. In this work we report a broadband room-temperature (RT) pulsed Fe:ZnSe laser tailored for highly-sensitive spectroscopic applications using the intracavity absorption spectroscopy (ICAS) technique [1], sometimes also called intracavity laser spectroscopy (ICLS), or intracavity laser absorption spectroscopy (ICLAS).

Compared to traditional spectroscopy techniques, ICAS offers a number of key advantages. In contrast to the conventional scheme *light source* → *sample* → *detector*, with ICAS the sample is placed inside the laser resonator. The successive interaction of laser photons with the broadband gain and the narrow-band absorption determines the laser emission spectrum. The laser light passes through the sample many times, resulting in large effective absorption path lengths of up to $L_{eff} = 7\times10^7$ m [2]. Depending on the gain medium and operation parameters of the laser, such processes as four-wave mixing, Rayleigh and Brillouin scattering can limit the sensitivity growth [1]. The laser generation time (measured from the very beginning of laser emission), after which no further increase in L_{eff} is observed, is referred to as the spectral saturation time t_s. Since an ICAS system reaches its maximum sensitivity at t_s, there is no advantage in operating a laser in CW mode. In pulsed operation mode with pulses shorter than t_s, the spectral sensitivity can be determined from the generation time t as $L_{eff} = ct$ [1], with c being the speed of light.

#422926 https://doi.org/10.1364/OE.422926
Journal © 2021 Received 16 Feb 2021; revised 29 Mar 2021; accepted 29 Mar 2021; published 1 Apr 2021

Optics EXPRESS

If the resonator is filled with the absorber only partially, a filling factor has to be considered additionally.

The most important advantage of ICAS compared to conventional absorption spectroscopy techniques is the ability to compensate broadband losses (e.g., light scattering and absorption by particles or by dirty windows of a technical apparatus, as well as beam steering) by the broadband gain medium. This mechanism makes ICAS unique and ideally suitable for measurements in challenging environments. Depending on the used laser medium, these broadband losses can be several tens of percent per roundtrip without significantly affecting the laser process, whereas with passive-cavity techniques, e.g. cavity ring-down spectroscopy (CRDS), broadband losses are not compensated and the light intensity decays fast below the noise level [3]. In contrast to the broadband losses, the narrow-band losses due to absorption by species under study are not compensated, such that the corresponding absorption lines are directly imprinted onto the laser emission spectrum. The latter process originates from mode-competition of the oscillating laser modes (frequencies) and is especially efficient when the homogeneous linewidth of the gain is larger than the absorption linewidth of the sample. This criterion is particularly fulfilled in solid-state lasers enabling accessing a broad spectrum of the sample(s) under study, thus facilitating multi-line and multi-species measurements.

As mentioned above, the effective absorption path length L_{eff} is an appropriate measure of the sensitivity with ICAS. Experimentally L_{eff} can be determined from the measured absorption signal K by using

$$K = \ln\left(\frac{I_0}{I}\right) = \ln\left(\frac{I_0}{I_0 \exp[-\alpha(\nu)L_{\mathrm{eff}}]}\right) = \alpha(\nu)L_{\mathrm{eff}}, \tag{1}$$

with I and I_0 being laser intensities with and without an absorber, respectively. The absorption coefficient $\alpha(\nu)$ of a sample (at wavenumber ν) is a product of the concentration n and the absorption cross-section $\sigma(\nu)$. Consequently, a determination of L_{eff} enables the subsequent calculation of unknown species concentrations or cross-sections from measured absorption signals.

Up to now, ICAS was employed in a wide range of hostile environments, including simultaneous concentration measurements of various molecular species in flames [4,5], identification and specification of chemical reactions in flames [6,7], simultaneous determination of temperature, pressure, and concentrations of gaseous samples in shock-tubes [8], measurements of absorption cross-sections of gas-phase FeO in a shock tube [9], monitoring of single transient processes in plasmas with microsecond time resolution [10], as well as simultaneous analysis of several isotopes of CO_2 in human breath [11]. However, despite these promising results achieved with ICAS in the visible and near-infrared in the recent years, there is still a great but largely unused potential for significant progress in this field, namely the advancement into the MIR spectral range, where the fundamental vibrational transitions of many species are located [12]. The present work makes a significant step towards the realization of this potential.

Due to great successes of quantum cascade lasers (QCLs) in the recent decades [13], they appear to be ideal candidates for ICAS in the MIR. However, the few works reported on ICAS with QCLs, e.g. at 7.5 µm in long-pulse (8 ms) operation [14] or around 8.1 µm in CW operation [15], demonstrated sensitivities that did not exceed $L_{\mathrm{eff}} = 50$ m, indicating a fundamental sensitivity limitation with QCLs. The underlying limiting mechanism is presumably the typically strong four-wave mixing [16], which enables QCL frequency combs, but is highly detrimental for ICAS since it suppresses the required mode competition. It should be noted that also for diode lasers a relatively low fundamental limit of $L_{\mathrm{eff}} \approx 10^4$ m has been found, with the main limiting mechanism being spontaneous emission [17].

In contrast to QCLs and diode lasers, sensitivities up to 10^7 m can be achieved with solid-state lasers (SSLs), as shown e.g. in [18]. However, up to now the reported SSL ICAS-systems addressed only the short-wavelength edge of MIR using either Co:MgF_2 lasers around 2 µm

Optics EXPRESS

[19–22], a Tm/Ho fiber laser around 2.1 µm [11], Cr:ZnSe lasers around 2.5 µm [23–26], or a color center laser around 2.7 µm [27], while only one work has spectroscopically investigated the deeper MIR by using a Fe:ZnSe laser at cryogenic temperatures for measurements of CH_4 around 4.1 µm [28]. The latter gain medium is of particular interest for ICAS.

Currently, lasers based on Fe^{2+}-doped chalcogenides provide access to the spectral range of 3.4–6.8 µm [29–31]. The employed host matrices include ZnTe [32], ZnS [29], CdSe [33], CdTe [34], ZnMnTe [35], ZnMnSe [36], ZnMgSe [37], and CdMnTe [38]. The best laser characteristics, however, have been obtained in Fe^{2+}-doped ZnSe crystals, usually lasing between 3.6 and 5.2 µm. Recent achievements include 1.1 kW peak power in Q-switched mode with a pulse duration of 20 ns and a repetition rate of 40 kHz [39], passive mode-locking with 732 fs pulses at a repetition rate of 100 MHz [40], CW output power of 9.2 W [41], efficiency of 59% [42], average power of 35 W at 100 Hz repetition rate [43], and an output energy of 10.6 J in single-shot operation [44].

Superior results with Fe:ZnSe lasers, however, can only be obtained at cryogenic temperatures, since the upper-laser-level lifetime increases with decreasing temperature from 0.37 µs at RT, to 60 µs at 80 K [45]. As a consequence, the limiting factor for energy up-scaling at RT is currently the lack of 3-µm high-energy short-pulse pump sources (while the relatively low threshold of laser-induced damage of ZnSe crystals also needs to be considered). Yet, the ongoing progress in the development of, e.g., Er:ZBLAN fiber lasers [46], and QCLs [47], is very promising for performance enhancement of RT Fe:ZnSe lasers. In this context an alternative pumping approach based on electron beams [48] is also worth mentioning. Despite the depicted limitations of RT Fe:ZnSe lasers, pulse energies of up to 1.67 J and average powers of 20 W have been demonstrated [49], which is sufficient for many practical applications, while avoiding complications associated with a cryostat.

Our current work presents a substantial advancement towards practical applications of MIR-ICAS in medical, atmospheric and combustion research. Compared to the Fe:ZnSe laser system reported in [28], our system improvements include: (i) room-temperature operation, (ii) laser resonator made of standard broadband aluminum mirrors instead of expensive dielectric mirrors with limited bandwidth, and (iii) the use of a pyroelectric camera for direct spectral recording instead of using the technically complex frequency-conversion into the visible range. Besides that, the long-wavelength penetration up to 5.29 µm is the deepest ever reported for Fe:ZnSe lasers, to the best of our knowledge.

From a spectroscopic point of view, the spectral range accessible by the Fe:ZnSe laser is very interesting since it contains absorption lines of such species as, e.g., NO, NO^+, N_2O, CO, CO_2, COF_2, CH_4, H_2O, H_2S, H_2CO, HBr, HI, O_3, OCS, SO_2 and PH_3 [12]. Highly-sensitive ICAS measurements of several of these species are demonstrated in this work.

2. Experimental setup

The experimental scheme of our laser system is depicted in Fig. 1. The cylindrical monocrystalline Fe^{2+}:ZnSe active element, 12 mm in diameter, 19 mm in length and a doping concentration of 1.6×10^{18} cm^{-3}, has been grown at the P.N. Lebedev Physical Institute of the Russian Academy of Sciences in Moscow using the modified vapor-phase method [50]. The laser resonator is formed by the two aluminum mirrors M1 ($r_1 = \infty$, plane-parallel) and M2 ($r_2 = 200$ mm), with the optical path inside the resonator of $L = 195$ mm. The Fe:ZnSe crystal is placed close to M1 under an angle of $\theta = 51°$ to the normal of M1, whereas the Brewster's angle is $\theta_B = 67.5°$.

On the one hand such crystal orientation prevents etalon fringes that are highly detrimental for ICAS, while on the other hand enables the outcoupling of ~5% of laser light reflected from the crystal's surface. This outcoupling is estimated to be sufficient for spectroscopic measurements using a home-made grating spectrograph (with a variable spectral resolution $\Delta\nu$ between 0.1 and 1 cm^{-1}) and the pyroelectric array camera PyroCam III HR (MKS/Ophir, 160×160 pixels, 12.8×12.8 mm^2 active area). Note that this resonator is not optimized with respect to inner losses,

Optics EXPRESS

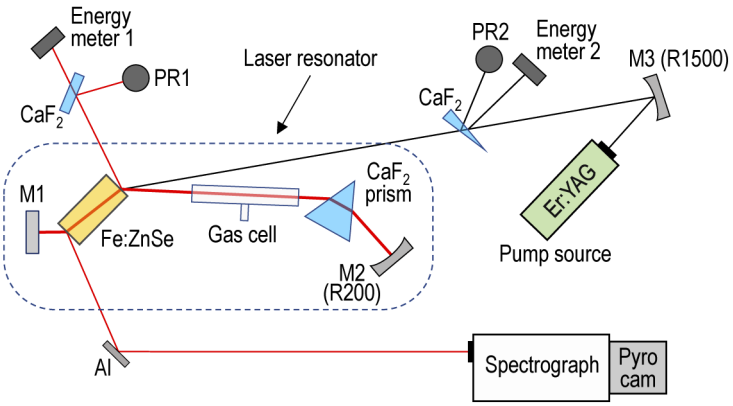

Fig. 1. Experimental setup.

due to the four reflections from the crystal surfaces per roundtrip. However, the utilized resonator scheme has the advantage of using standard (broadband) aluminum mirrors instead of expensive and typically bandwidth-limited dielectric mirrors.

An open tube (gas cell) with a diameter of $d = 15$ mm and a length of $l = 75$ mm is installed in the resonator for ICAS measurements in human breath and in gas flows of N_2O (diluted in N_2). The resulting filling factor of the resonator is $l/L = 38.5\%$, however, since the gas flows go slightly beyond the tube edges, a filling factor of 40% is assumed in the following calculations. A CaF_2 prism (70°) is used for spectral tuning of the laser. The reflection from the crystal's second surface is utilized for pulse-energy (energy meter 1 in Fig. 1) and pulse-shape (photoresistor PR1) monitoring, which have already been described in detail [31].

As a pump source we use a home-made 40-ns (FWHM) Q-switched Er:YAG laser emitting up to 40 mJ at 2.94 µm, and operating in the single-pulse regime. The pump light is focused onto the laser crystal using the aluminum mirror M3 with a radius of curvature of $r = 1500$ mm. For higher flexibility in adjusting the Fe:ZnSe laser, a pump-spot diameter of 2 mm is utilized. A CaF_2 wedge is used as a 3%-deflector for pulse-energy (energy meter 2 in Fig. 1) and pulse-shape (PR2) characterization. The pump laser is synchronized with the pyroelectric camera using a pulse generator (not shown in Fig. 1).

3. Characterization of the system

The input-output characteristics of the Fe:ZnSe laser operating around the gain maximum at 4.4 µm are shown in Fig. 2. The achieved slope efficiency with respect to the incident pump energy is $\eta = 2.4\%$, while the laser threshold is about 1 mJ. It should be noted that the measured laser output energy originates from the reflection of one crystal-surface (cf. Fig. 1). The inset of Fig. 2 shows the pulse shapes of the Er:YAG (orange) and the Fe:ZnSe (green) lasers.

The spectral tuning of the Fe:ZnSe laser is performed by using an intracavity CaF_2 prism and incrementally tilting M2. The achieved tuning range of our laser is shown in Fig. 3.

Each experimental spectrum (bottom) has been recorded at a fixed tilt of M2. As can be seen, the Fe:ZnSe is continuously tunable in the spectral range of 1890–2660 cm^{-1} (3.76–5.29 µm). The long-wavelength edge is the longest reported up to now for a Fe:ZnSe laser, to the best of our knowledge. The colored spectra (Fig. 3, bottom) have been recorded with a spectral resolution of $\Delta\nu = 0.3$ cm^{-1}. The wavelength calibration has been performed using well-known line positions (HITRAN database [12]) of either atmospheric H_2O and CO_2, or by introducing gas flows with suitable concentration of N_2O into the open gas cell located inside the resonator. Figure 3 (top) shows calculated transmission spectra for air containing typical 0.8% of H_2O

Optics EXPRESS

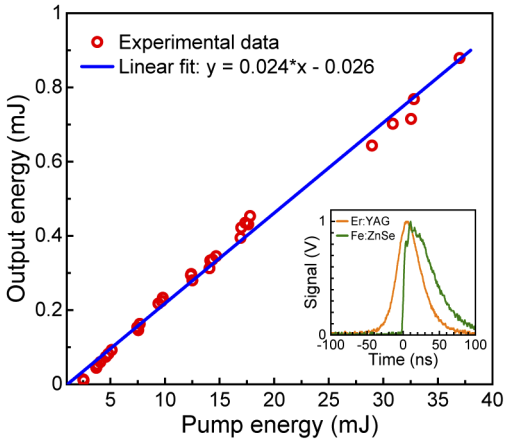

Fig. 2. Input-output characteristics of the Fe:ZnSe laser. The inset shows the temporal profiles of the pump (orange) and laser (green) pulses.

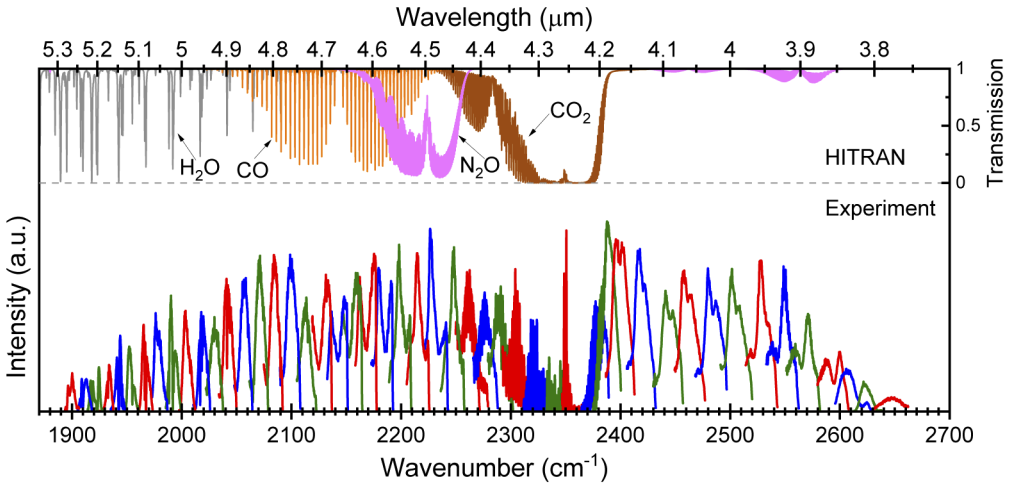

Fig. 3. Tuning range of the Fe:ZnSe laser (bottom) recorded with a spectral resolution of $\Delta\nu = 0.3$ cm^{-1}. A spectral shift (color change) corresponds to an incremental tilt of mirror M2. Calculated transmission spectra (HITRAN) of atmospheric H_2O (grey) and CO_2 (brown), as well as of 100 ppm of N_2O (pink) and 50 ppm of CO (orange), are shown on top.

Optics EXPRESS

(grey) and 0.04% of CO_2 (brown), as well as an N_2O spectrum with a concentration of 0.01% (pink) and a spectrum of 0.005% of CO (orange), in all cases assuming an effective absorption path length of $L_{eff} = 10$ m. As can be seen, a large part of the Fe:ZnSe tuning range laser is free of atmospheric absorption by H_2O and CO_2, thus enabling corresponding field applications.

Due to the limited sensor size of the pyroelectric camera, only a fraction of an individual spectrum can be recorded at the chosen spectral resolution of 0.3 cm^{-1}. To record a full individual spectrum of the Fe:ZnSe laser (i.e. at a fixed position of mirror M2), we have reduced the spectral resolution to $\Delta\nu = 1$ cm^{-1} (by reducing the dispersion). The results are shown in Fig. 4. The brown emission spectrum of the Fe:ZnSe laser is an average of 16 single-shot spectra and has been recorded in air. After that, a smoldering paper has been placed inside the resonator and a spectrum of its smoke has been recorded (blue in Fig. 4). A comparison of the normalized experimental spectrum (red) with a calculated HITRAN spectrum of 70 ppm of CO (green, $L_{eff} = 10$ m) shows that almost all absorption lines in the experimental spectrum originate from CO. Furthermore, as can be seen, a total spectral range of ~60 cm^{-1} can be monitored simultaneously, i.e. without tuning the laser, which is very advantageous for single-shot spectroscopic applications, e.g., in shock-tubes. These results demonstrate the multi-line (or multi-species) capabilities of broadband ICAS.

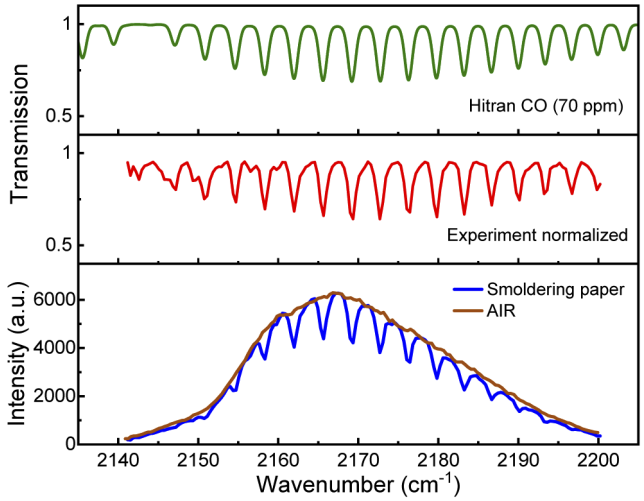

Fig. 4. Bottom: individual emission spectra of the Fe:ZnSe laser recorded with a spectral resolution of $\Delta\nu = 1$ cm^{-1} in air (brown) and with a smoldering paper inside the resonator (blue). Center: normalized experimental spectrum. Top: a calculated spectrum of 70 ppm of CO (HITRAN).

4. ICAS of CO_2 isotopes in atmosphere and in human breath

Measurements of CO_2 isotopes are important in various research fields such as, e.g., environmental sciences [51], archeology [52], minerology [53], medicine [54] and astronomy [55]. The development of optical detection techniques enabled significant progress and new insights in all these fields. As will be shown in this section, the Fe:ZnSe-laser based ICAS system is capable to extend the existing spectroscopic toolbox and enable new applications.

4.1. Measurements of atmospheric CO_2

Spectroscopic measurements of atmospheric CO_2 have been performed with a spectral resolution of $\Delta\nu = 0.1$ cm^{-1}, which is also considered in calculations using the HITRAN database. The

Optics EXPRESS

Fe:ZnSe laser has been tuned to the spectral range around 2300 cm^{-1} and a series of six overlapping spectra (each averaged over 25 single-shot spectra) has been recorded by stepwise tuning the spectrometer. Subsequently, the experimental spectra have been normalized by the spectral envelope (obtained by polynomial fitting of laser intensities without absorption) and combined to one spectrum as described in [4]. The result is shown in Fig. 5 in blue.

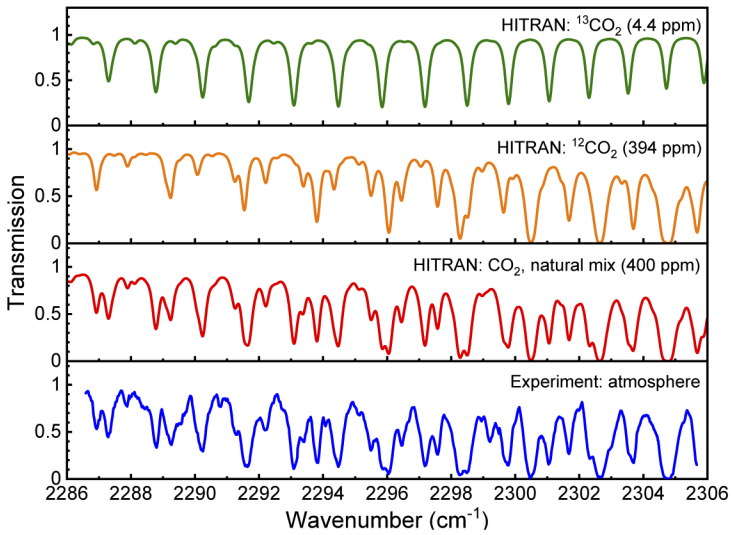

Fig. 5. Normalized and combined experimental spectrum with intracavity absorption of atmospheric CO_2 (blue, $\Delta\nu = 0.1$ cm^{-1}) shows good agreement with the calculated spectrum of CO_2 (red, 400 ppm, natural mix). For comparison, calculated spectra of the two main isotopes, $^{12}CO_2$ and $^{13}CO_2$, are also shown.

The experimental spectrum shows a good agreement with the fitted spectrum of atmospheric CO_2 (red, natural mix, 400 ppm) from the HITRAN database. In the fitting process, the effective absorption path length L_{eff} has been varied and the best-fit result was obtained with $L_{\text{eff,tot}} = 13$ m by visually comparing the overlapped experimental and theoretical spectra. The accuracy with this procedure is about ±5%. Considering the optical distance between the laser and the pyroelectric detector of 7.2 m (resulting from 1.1 m between laser and spectrometer and 6.1 m inside the spectrometer), the effective absorption path length accumulated inside the resonator is $L_{\text{eff}} = 5.8$ m. Provided a narrow (e.g. below 1 ns) detection window and a corresponding sensitivity of the pyroelectric camera, this L_{eff} could be achieved at a laser generation time of $t = L_{\text{eff}}/c \approx 20$ ns. However, due to the low sensitivity of our pyroelectric camera, the whole laser pulse has to be integrated during a spectral recording. As a consequence, the integrated absorption signal has a complex dependence on the absorption coefficient [56] and Eq. (1) needs to be modified to

$$K = \ln\left(\frac{\int_0^T I_0(t)\,\mathrm{d}t}{\int_0^T I_0(t)\ \exp[-\alpha(\nu)\ c\ t]\,\mathrm{d}t}\right), \tag{2}$$

with $I_0(t)$ being the laser pulse shape shown in Fig. 2 and (T) being the laser pulse duration. From Eq. (2) it becomes clear, that high-intensity parts of a laser pulse have a stronger contribution to the integrated absorption signal than low-intensity parts. The specific pulse shape of our laser suggests a strong shift of the mean generation time towards smaller values and $t = 20$ ns fits well into these considerations.

Optics EXPRESS

Figure 5 also shows individual calculated spectra of the two main isotopes of CO_2, namely $^{12}CO_2$ (orange) and $^{13}CO_2$ (green). Note, that although the concentrations of the two isotopes differ by two orders of magnitude, their absorption signals in this spectral region are comparable. Consequently, the Fe:ZnSe laser is suitable for highly sensitive simultaneous measurements of both isotopes. With the estimated noise level in the experimental spectra of about 2% (RMS), a noise-equivalent detection limit for the strongest $^{12}CO_2$ absorption line at 2361.46 cm^{-1} is estimated to be $p_{min,12CO2} = 110$ ppb, while for the strongest line of $^{13}CO_2$ at 2295.85 cm^{-1} the detection limit is about $p_{min,13CO2} = 100$ ppb.

A similar estimate can be made for atmospheric H_2O. The detection limit for the strongest line located at 1918.2 cm^{-1} is $p_{min,H2O} = 8$ ppm.

4.2. Measurements of CO_2 isotopes in human breath

Breath gas analysis is a promising approach for non-invasive medical diagnostics and physiological monitoring [57]. This section demonstrates the possibilities of the Fe:ZnSe-laser based ICAS-system for breath analysis of CO_2.

4.2.1. ICAS of $^{12}CO_2$ and $^{13}CO_2$ in breath

After the determination of the effective absorption path length ($L_{eff} = 5.8$ m), the ICAS system is fully characterized and can be applied to more elaborate measurements. As the first such application we have chosen the in-situ breath analysis of CO_2. For this purpose, the laser is tuned to the spectral range of 2225 cm^{-1}, which is free of atmospheric absorption, and a series of five overlapping spectra (each 25-fold averaged) is recorded by stepwise tuning the spectrometer. In the experiment, the test person breathes out through a hose into the open tube placed inside the laser cavity. It should be noted that the previously determined effective absorption path length of 5.8 m needs to be corrected by the filling factor of the cavity with the open tube of 40%,

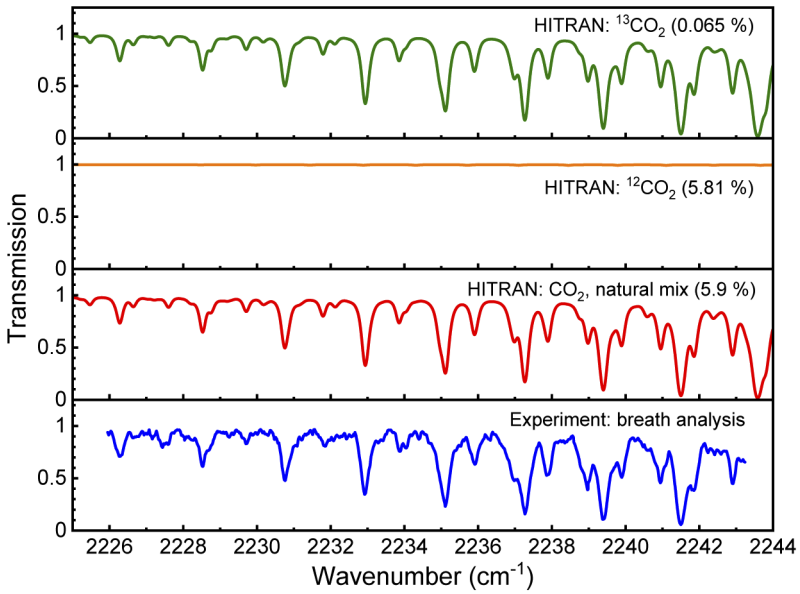

Fig. 6. Experimental spectrum with intracavity absorption of breath CO_2 (blue, $\Delta\nu = 0.1$ cm^{-1}) shows good agreement with the calculated spectrum of CO_2 (red, 5.9%, natural mix). Almost the entire absorption originates from the isotope $^{13}CO_2$, as shown by calculated spectra of the isotopes $^{12}CO_2$ (orange) and $^{13}CO_2$ (green).

Optics EXPRESS

resulting in $L_{\text{eff}} = 2.3$ m. The recorded breath-spectra are normalized by spectra recorded in air and combined to one spectrum. Subsequently, the combined spectrum is evaluated by fitting HITRAN spectra of CO_2 (natural mix), with the CO_2 concentration being the fit parameter. The results are shown in Fig. 6.

The best-fit concentration of CO_2 is determined to be 5.9%, which is within the usual range of 5–6% during an exhalation [58]. The corresponding spectrum is shown in Fig. 6 in red. As can be seen, the experimental and calculated spectra are in good agreement for all spectral features. A calculation of corresponding spectra of the two main isotopes of CO_2, namely $^{12}CO_2$ (orange) and $^{13}CO_2$ (green), reveals that almost the entire absorption originates from the 0.065% of $^{13}CO_2$ in breath. However, it is also worth taking a closer look on other isotopes and quantify their contribution. This is addressed theoretically in the following subsection.

4.2.2. Feasibility of $^{16}O^{13}C^{18}O$ measurements

Figure 7 shows calculated (HITRAN) absorption coefficients of the first five isotopes of CO_2, being $^{12}CO_2$, $^{13}CO_2$, $^{16}O^{12}C^{18}O$, $^{16}O^{12}C^{17}O$ and $^{16}O^{13}C^{18}O$, in the spectral range of 2200–2400 cm^{-1}.

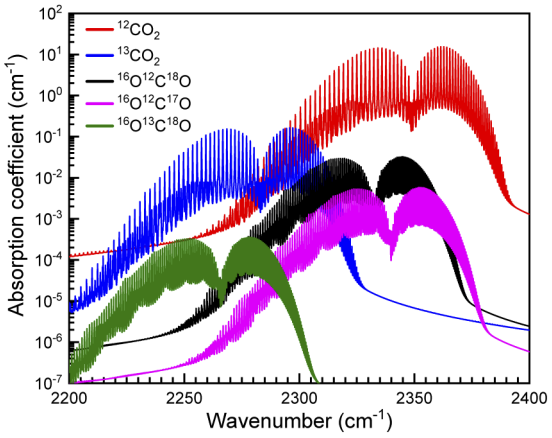

Fig. 7. Absorption coefficients of the first five isotopes of CO_2.

The calculation is performed with a typical breath-CO_2 concentration of 6%, using the isotopic abundance provided in the HITRAN database. As can be seen, the locations of spectral bands of the third (black in Fig. 7) and fourth (pink) isotopes almost fully coincide with the main isotope, which has 3–4 orders of magnitude higher absorption coefficient, thus making a detection of $^{16}O^{12}C^{18}O$ and $^{16}O^{12}C^{17}O$ very challenging. In contrast, the spectrum of the isotope $^{16}O^{13}C^{18}O$ (green) is shifted towards lower wavenumbers, even further than the isotope $^{13}CO_2$ (blue). As a consequence, between 2200 and 2250 cm^{-1} the absorption coefficients of the two latter isotopes differ by only two orders of magnitude, thus facilitating a detection of $^{16}O^{13}C^{18}O$, as illustrated by a calculation in Fig. 8.

As can be seen, the presence of the isotope $^{16}O^{13}C^{18}O$ is characterized by distinct absorption features marked by arrows in Fig. 8. These calculations show that $^{16}O^{13}C^{18}O$ can be detected in this spectral range despite the two orders of magnitude lower absorption coefficient.

The isotope $^{16}O^{13}C^{18}O$ plays an important role in geochemistry [59] and only recently the possibility of its detection using an optical technique (instead of mass-spectrometry) has been demonstrated [60]. Our current work illustrates that the ICAS system based on the Fe:ZnSe laser is also well suitable for this purpose. The absorption signals of $^{16}O^{13}C^{18}O$ in Fig. 8 are on the order of the noise level (2%). Since the main spectral noise component with broadband

Optics EXPRESS

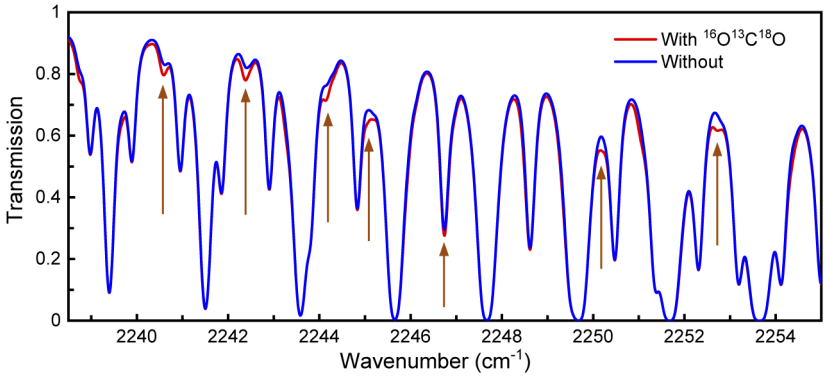

Fig. 8. Calculated transmission spectra of CO_2, including the isotope $^{16}O^{13}C^{18}O$ (red) and without it (blue), for typical concentrations in breath and $L_{eff} = 2.3$ m.

(multi-mode) lasers is random [1,61], it can be reduced by averaging over spectra of consecutive laser pulses and/or over intensities of neighboring laser modes [10]. Therefore, at least a factor of 10 in noise reduction is expected, thus facilitating the detection of $^{16}O^{13}C^{18}O$. One of the advantages of our system is the capability of simultaneously monitoring a broad spectral range, thus enabling higher accuracy in comparison with the single-line monitoring around $\nu = 2252.7$ cm^{-1} reported in [60]. Besides that, the detection-sensitivity of $L_{eff} = 10$ m in the latter works has been achieved by using a multi-pass cell, which is limited by the physical dimensions of the gas cell. In contrast, with ICAS the sensitivity can be increased by increasing the pulse duration of the laser.

Typically, the saturation time of sensitivity-growth for solid-state lasers is in the ms range, corresponding to several 10^6 m of absorption path length, as e.g. shown for a Cr:forsterite laser [18], or for a Cr:ZnSe laser [26]. These examples clearly demonstrate the feasibility of enhancement factors in L_{eff} on the order of 10^6 for the Fe:ZnSe laser. In our current setup, the sensitivity is limited by the fixed 40-ns pulse-width of the Er:YAG pump source. However, 300-µs pulses of a Fe:ZnSe laser have already been demonstrated in [62], with the crystal slightly cooled to 5 °C using a Peltier-element. The required threshold pump power-density was about 17 kW/cm^2. This value can be surpassed by using e.g. a recently emerged commercially available 10-W Er:ZBLAN fiber laser operating at 2.9 µm. Due to the excellent beam quality of the fiber laser, a focusing spot diameter of e.g. 0.1 mm can be easily achieved, thus providing about 130 kW/cm^2. These considerations clearly prove the feasibility of ms-pulses of the Fe:ZnSe laser at RT. Consequently, the route for further progress in ICAS in the MIR spectral range is straightforward. In particular, the proposed enhancement in L_{eff} and noise reduction are expected to increase the current sensitivity by up to a factor of 10^7, resulting in CO_2 detection limits in the range of parts per quadrillion (ppq).

5. ICAS of N_2O in a gas flow

Nitrous oxide (N_2O) is an important greenhouse gas, with a 300-times larger global warming potential than CO_2 [63]. In this context, the recently demonstrated optical detection of up to 7 isotopes of N_2O using a multi-pass cell ($L_{eff} = 204$ m) and QCLs around 2142 and 2182 cm^{-1} [64] is very interesting.

As can be seen from Fig. 2, the emission range of the Fe:ZnSe laser is also nicely suitable for highly-sensitive detection of N_2O, enabling measurements of its various bands. To perform measurements of N_2O in a gas flow, the open gas cell inside the laser resonator has been connected to a gas bottle containing a mixture of about 0.01% of N_2O in N_2. Since the mixture has been

Optics EXPRESS

prepared on-site, the exact gas proportions were not known prior to the ICAS measurements. A constant gas flow has been adjusted by manually regulating the bottle valve. Similar to the procedure described above for CO_2 measurements, five overlapping spectra (each 25-fold averaged) have been recorded by stepwise tuning the spectrometer. The normalized and combined spectrum of N_2O is shown in Fig. 9 in blue, together with a calculated spectrum using the HITRAN database (red).

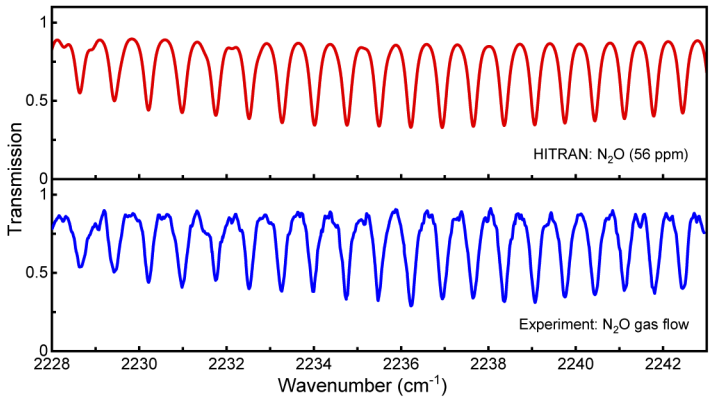

Fig. 9. The experimental spectrum of N_2O (blue, $\Delta\nu = 0.1$ cm^{-1}) recorded in a gas flow shows good agreement with a calculated spectrum of N_2O (56 ppm) from the HITRAN database.

The HITRAN calculation has been performed using the experimental parameters of $p_{tot} = 1$ bar, $L_{eff} = 2.3$ m, $\Delta\nu = 0.1$ cm^{-1} and varying the N_2O partial pressure until the best agreement with the experimental spectrum has been achieved at $p_{N2O} = 56$ ppm. It can be seen that experiment and calculation agree well in the whole spectral range under study. With this, the prepared mixture concentration has been determined to be 56 ppm of N_2O in N_2. The estimated detection limit for the strongest N_2O line at 2295.85 cm^{-1} is about $p_{min,N2O} = 1$ ppm. With an implementation of the proposed system improvements described in the previous section (noise reduction and especially enhancement of L_{eff}), the detection limit may be reduced by about 7 orders of magnitude down to the ppq level.

6. Measurements of CO in human breath after cigarette smoking

Carbon monoxide is a well-known combustion product, however, in breath analysis it also serves as a biomarker of oxidative stress, respiratory infections and asthma [65,66]. Typical concentrations in the breath of non-smokers are on the order of several ppm, whereas the CO concentrations in smokers are typically 1–2 orders of magnitude higher [67]. Recently, an important advancement in using optical techniques for real-time breath analysis of two isotopes of CO has been demonstrated in the 2130 cm^{-1} spectral range (4.69 μm) using interband cascade lasers [68]. Since the Fe:ZnSe also covers this spectral range, breath analysis of CO is another possible application of our spectroscopic system.

As a demonstration, we have measured CO in human breath, before and immediately after smoking a cigarette. The measurement protocol was as follows: the test person was asked to breathe out through a hose connected to the open tube located inside the laser resonator while an 25-fold averaged laser emission spectrum has been recorded. Subsequently, the test person smoked a cigarette and was then asked to breathe through the hose again. For comparison, a spectrum with a smoldering piece of paper located in the resonator has also been recorded. In contrast to measurements presented in previous sections, here only one spectrum at a fixed

Optics EXPRESS

position of the spectrometer has been recorded. The normalized experimental spectra and a calculated spectrum of CO (HITRAN) are shown in Fig. 10.

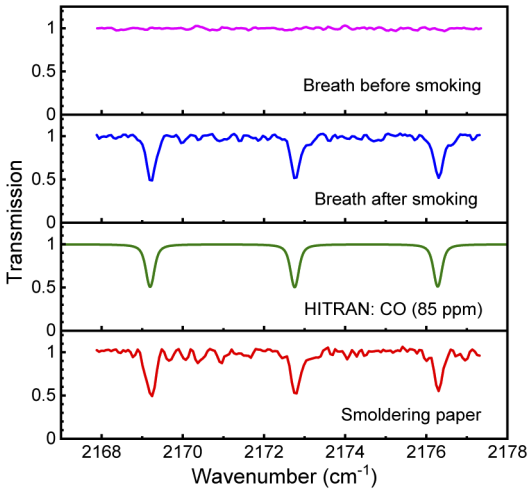

Fig. 10. Experimental spectra recorded with a spectral resolution of $\Delta\nu = 0.15$ cm^{-1} in breath after cigarette smoking (blue) and with a smoldering paper in the resonator (red) showing good agreement with a calculated spectrum of CO (green, 85 ppm) from the HITRAN database.

As can be seen, the breath spectrum recorded before smoking a cigarette (pink) does not contain any absorption lines above the noise level of 2% (RMS). It can be concluded that the sensitivity of our current system is insufficient for detecting CO in breath (due to the limited pump-pulse duration of 40 ns). However, distinct absorption lines can be observed in the spectrum recorded after smoking a cigarette (blue). A comparison with the calculated spectrum of CO (green in Fig. 10, $L_{\text{eff}} = 2.3$ m, $\Delta\nu = 0.15$ cm^{-1}) shows that the large absorption lines in the blue spectrum originate from CO and the concentration is about 85 ppm. The spectrum recorded in the smoke of a smoldering paper (red) shows almost the same absorption-line depths, however, the concentration in this case is not precisely determined since it is not clear which part of the cavity is filled with the absorber. When assuming a complete filling of the cavity, the corresponding CO concentration is about 33 ppm.

In addition to the absorption by CO, some smaller absorption lines can be observed in the blue and red experimental spectra, especially pronounced in the spectrum of the smoldering paper. However, the corresponding combustion products could not be identified yet.

The estimated detection limit for the strongest CO line at 2172.76 cm^{-1} is about $p_{\text{min,CO}} = 3$ ppm for the blue spectrum, which is slightly higher than the typical breath CO concentration of 1.2 ppm in non-smokers [65]. The above described noise reduction and enhancement of L_{eff} should result in a detection limit on the ppq level, enabling extremely sensitive measurements of CO in various environments.

7. Conclusion

This work demonstrates a two-fold progress in the development of Fe:ZnSe lasers. First, we have obtained the longest-wavelength emission from a Fe:ZnSe laser of up to 5.29 µm, whereas previously reported systems were limited by about 5.2 µm. Second, a significant step towards the realization of the Fe:ZnSe laser's potential as a MIR spectroscopic tool is made. In particular, we built up a room-temperature setup for intracavity absorption spectroscopy and employed a laser cavity based on standard (broadband) aluminum mirrors instead of bandwidth-limited

Optics EXPRESS

dielectric mirrors. Our system is continuously tunable in the spectral range of 3.76–5.29 µm, which contains strong absorption lines of dozens of species. The spectral bandwidth of individual laser emission spectra is about 60 cm^{-1}, enabling multi-line or multi-species detection. We demonstrate broadband and sensitive measurements of different isotopes of atmospheric and breath CO_2, breath CO after smoking a cigarette, CO from a smoldering paper, and N_2O in a gas flow. The sensitivity of the developed ICAS system currently corresponds to an effective absorption path length of $L_{eff} = 5.8$ m (for a cavity entirely filled with the absorber). Nevertheless, the achieved detection limits are: 0.1 ppm for $^{12}CO_2$ and $^{13}CO_2$, 1 ppm for N_2O, 3 ppm for CO, as well as 8 ppm for atmospheric H_2O. The sensitivity of the current setup is limited by the short pump-pulse duration of 40 ns. However, by employing the recently emerged commercial availability of CW Er:ZBLAN fiber lasers as a pump source, a sensitivity enhancement by a factor of about 10^6 is expected. Combined with a factor 10 lower spectral noise level achievable through a higher number of averages, this will enable ultra-low detection limits on the order of parts per quadrillion (ppq). The presented work is a significant step towards the realization of broadband ultra-sensitive room-temperature ICAS systems in the MIR spectral range.

Funding. Russian Academy of Sciences (Program No. 5); Deutsche Forschungsgemeinschaft (Research Unit 2284, project 262219004); Russian Science Foundation (20-79-00155).

Acknowledgments. The authors wish to thank V.M. Baev for helpful discussions. P. Fjodorow acknowledges the support by the PRIME program of the German Academic Exchange Service (DAAD), funded by the German Federal Ministry of Education and Research (BMBF). We acknowledge the support by the Open Access Publication Fund of the University of Duisburg-Essen. S.O. Leonov acknowledges the Russian Science Foundation for the support in the measurements of laser spectra.

Disclosures. The authors declare that there are no conflicts of interest related to this article.

Data availability. Data underlying the results presented in this paper are not publicly available at this time but may be obtained from the authors upon reasonable request.

References

1. V. M. Baev, T. Latz, and P. E. Toschek, "Laser intracavity absorption spectroscopy," Appl. Phys. B **69**(3), 171–202 (1999).
2. J. Sierks, T. Latz, V. M. Baev, and P. E. Toschek, "Spectral dynamics of multi-mode dye lasers and single-atom absorption," in *International Quantum Electronics Conference, 1996 OSA Technical Digest Series* (Optical Society of America, 1996), paper FC6.
3. I. Rahinov, A. Goldman, and S. Cheskis, "Intracavity laser absorption spectroscopy and cavity ring-down spectroscopy in low-pressure flames," Appl. Phys. B **81**(1), 143–149 (2005).
4. B. Löhden, S. Kuznetsova, K. Sengstock, V. M. Baev, A. Goldman, S. Cheskis, and B. Pálsdóttir, "Fiber laser intracavity absorption spectroscopy for in situ multicomponent gas analysis in the atmosphere and combustion environments," Appl. Phys. B **102**(2), 331–344 (2011).
5. I. Rahinov, A. Goldman, and S. Cheskis, "Absorption spectroscopy diagnostics of amidogen in ammonia-doped methane/air flames," Combust. Flame **145**(1-2), 105–116 (2006).
6. F. Stoeckel, M. D. Schuh, N. Goldstein, and G. H. Atkinson, "Time-resolved intracavity laser spectroscopy: 266 nm photodissociation of acetaldehyde vapor to form HCO," Chem. Phys. **95**(1), 135–144 (1985).
7. P. Sheehy and J. I. Steinfeld, "Discharge–Flow Kinetics Measurements Using Intracavity Laser Absorption Spectroscopy," J. Phys. Chem. B **109**(17), 8358–8362 (2005).
8. P. Fjodorow, M. Fikri, C. Schulz, O. Hellmig, and V. M. Baev, "Time-resolved detection of temperature, concentration, and pressure in a shock tube by intracavity absorption spectroscopy," Appl. Phys. B **122**(6), 159 (2016).
9. P. Fjodorow, M. R. Lalanne, D. He, M. Nanjaiah, A. Pilipodi-Best, V. M. Baev, S. Cheskis, J. Herzler, M. Fikri, I. Wlokas, C. Schulz, and I. Rahinov, "Determination of gas-phase absorption cross-sections of FeO in a shock tube using intracavity absorption spectroscopy near 611 nm," Proc. Combust. Inst. **38**(1), 1637–1645 (2020).
10. P. Fjodorow, I. Baev, O. Hellmig, K. Sengstock, and V. M. Baev, "Sensitive, time-resolved, broadband spectroscopy of single transient processes," Appl. Phys. B **120**(4), 667–673 (2015).
11. P. Fjodorow, O. Hellmig, and V. M. Baev, "A broadband Tm/Ho-doped fiber laser tunable from 1.8 to 2.09 µm for intracavity absorption spectroscopy," Appl. Phys. B **124**(4), 62 (2018).
12. I. E. Gordon, L. S. Rothman, C. Hill, R. V. Kochanov, Y. Tan, P. F. Bernath, M. Birk, V. Boudon, A. Campargue, K. V. Chance, B. J. Drouin, J. M. Flaud, R. R. Gamache, J. T. Hodges, D. Jacquemart, V. I. Perevalov, A. Perrin, K. P. Shine, M. A. H. Smith, J. Tennyson, G. C. Toon, H. Tran, V. G. Tyuterev, A. Barbe, A. G. Császár, V. M. Devi, T. Furtenbacher, J. J. Harrison, J. M. Hartmann, A. Jolly, T. J. Johnson, T. Karman, I. Kleiner, A. A. Kyuberis, J. Loos, O. M. Lyulin, S. T. Massie, S. N. Mikhailenko, N. Moazzen-Ahmadi, H. S. P. Müller, O. V. Naumenko, A. V.

Optics EXPRESS

Nikitin, O. L. Polyansky, M. Rey, M. Rotger, S. W. Sharpe, K. Sung, E. Starikova, S. A. Tashkun, J. V. Auwera, G. Wagner, J. Wilzewski, P. Wcisło, S. Yu, and E. J. Zak, "The HITRAN2016 molecular spectroscopic database," J. Quant. Spectrosc. Radiat. Transfer **203**, 3–69 (2017).

13. M. S. Vitiello, G. Scalari, B. Williams, and P. De Natale, "Quantum cascade lasers: 20 years of challenges," Opt. Express **23**(4), 5167–5182 (2015).
14. M. C. Phillips and M. S. Taubman, "Intracavity sensing via compliance voltage in an external cavity quantum cascade laser," Opt. Lett. **37**(13), 2664–2666 (2012).
15. A. V. Muraviev, D. E. Maukonen, C. J. Fredricksen, G. Medhi, and R. E. Peale, "Quantum cascade laser intracavity absorption spectrometer for trace gas sensing," Appl. Phys. Lett. **103**(9), 091111 (2013).
16. P. Friedli, H. Sigg, B. Hinkov, A. Hugi, S. Riedi, M. Beck, and J. Faist, "Four-wave mixing in a quantum cascade laser amplifier," Appl. Phys. Lett. **102**(22), 222104 (2013).
17. V. M. Baev, J. Eschner, E. Paeth, R. Schüler, and P. E. Toschek, "Intra-cavity spectroscopy with diode lasers," Appl. Phys. B **55**(6), 463–477 (1992).
18. P. Fjodorow, S. Löhden, O. Hellmig, C. Schulz, and V. M. Baev, "A Cr^{4+}:forsterite laser for intracavity absorption spectroscopy in the spectral range of 1.2-1.4 µm," Opt. Express **27**(8), 11122–11136 (2019).
19. M. P. Frolov and Y. P. Podmar'kov, "Intracavity laser spectroscopy with a Co:MgF_2 laser," Opt. Commun. **155**(4-6), 313–316 (1998).
20. Y. P. Podmar'kov, N. A. Raspopov, A. N. Savchenko, and M. P. Frolov, "Dynamics of the intracavity absorption in the spectrum of a Co:MgF_2 laser emitting for up to 1 ms," Quantum Electron. **29**(3), 223–225 (1999).
21. Y. P. Podmar'kov, N. A. Raspopov, A. N. Savchenko, and M. P. Frolov, "Highly sensitive detection of gaseous impurities by intracavity laser spectroscopy based on a Co:MgF_2 laser," Quantum Electron. **29**(8), 742–744 (1999).
22. N. P. Vagin, A. A. Ionin, I. V. Kochetov, A. P. Napartovich, Y. P. Podmar'kov, M. P. Frolov, and N. N. Yuryshev, "Measurement of the $O_2(b^1\Sigma_g^+ \rightarrow a^1\Delta_g)$ transition probability by the method of intracavity laser spectroscopy," Quantum Electron. **35**(4), 378–384 (2005).
23. V. A. Akimov, V. I. Kozlovskii, Y. V. Korostelin, A. I. Landman, Y. P. Podmar'kov, and M. P. Frolov, "Intracavity laser spectroscopy using a Cr^{2+}:ZnSe laser," Quantum Electron. **34**(2), 185–188 (2004).
24. N. Picqué, F. Gueye, G. Guelachvili, E. Sorokin, and I. T. Sorokina, "Time-resolved Fourier transform intracavity spectroscopy with a Cr^{2+}:ZnSe laser," Opt. Lett. **30**(24), 3410–3412 (2005).
25. V. A. Akimov, V. I. Kozlovskii, Y. V. Korostelin, A. I. Landman, Y. P. Podmar'kov, and M. P. Frolov, "Spectral dynamics of intracavity absorption in a pulsed Cr^{2+}:ZnSe laser," Quantum Electron. **35**(5), 425–428 (2005).
26. V. I. Kozlovsky, Y. V. Korostelin, O. G. Okhotnikov, Y. P. Podmar'kov, Y. K. Skasyrsky, M. P. Frolov, and V. A. Akimov, "Intracavity laser spectroscopy with a semiconductor disk laser-pumped cw Cr^{2+}:ZnSe laser," Quantum Electron. **43**(9), 885–889 (2013).
27. V. M. Baev, V. P. Dubov, A. N. Kireev, E. A. Sviridenkov, D. D. Toptygin, and O. I. Yushchuk, "Application of lasers withFA(II) color centers in KCl:Li crystals in intracavity laser spectroscopy," Quantum Electron. **16**(8), 1121–1123 (1986).
28. V. A. Akimov, A. A. Voronov, V. I. Kozlovskii, Y. V. Korostelin, A. I. Landman, Y. P. Podmar'kov, and M. P. Frolov, "Intracavity laser spectroscopy by using a Fe^{2+}:ZnSe laser," Quantum Electron. **37**(11), 1071–1075 (2007).
29. M. P. Frolov, Y. V. Korostelin, V. I. Kozlovsky, Y. P. Podmar'kov, S. A. Savinova, and Y. K. Skasyrsky, "3 J pulsed Fe:ZnS laser tunable from 3.44 to 4.19 µm," Laser Phys. Lett. **12**(5), 055001 (2015).
30. S. B. Mirov, I. S. Moskalev, S. Vasilyev, V. Smolski, V. V. Fedorov, D. Martyshkin, J. Peppers, M. Mirov, A. Dergachev, and V. Gapontsev, "Frontiers of Mid-IR Lasers Based on Transition Metal Doped Chalcogenides," IEEE J. Sel. Top. Quantum Electron. **24**(5), 1–29 (2018).
31. M. P. Frolov, Y. V. Korostelin, V. I. Kozlovsky, S. O. Leonov, and Y. K. Skasyrsky, "Tunable in the range of 4.5–6.8 µm room temperature single-crystal Fe:CdTe laser pumped by Fe:ZnSe laser," Opt. Express **28**(12), 17449–17456 (2020).
32. M. P. Frolov, Y. V. Korostelin, V. I. Kozlovsky, V. V. Mislavsky, Y. P. Podmar'kov, Y. K. Skasyrsky, and A. A. Voronov, "Laser radiation tunable within the range of 4.35–5.45 µm in a ZnTe crystal doped with Fe^{2+} ions," J. Russ. Laser Res. **32**(6), 528–536 (2011).
33. M. P. Frolov, V. M. Gordienko, Y. V. Korostelin, V. I. Kozlovsky, Y. P. Podmar'kov, F. V. Potemkin, and Y. K. Skasyrsky, "Fe^{2+}-doped CdSe single crystal: growth, spectroscopic and laser properties, potential use as a 6 µm broadband amplifier," Laser Phys. Lett. **14**(2), 025001 (2017).
34. M. P. Frolov, Y. V. Korostelin, V. I. Kozlovsky, S. O. Leonov, P. Fjodorow, and Y. K. Skasyrsky, "Efficient Fe:CdTe laser producing 0.35 J pulses in the 5 µm spectral range," Opt. Lett. **45**(24), 6647–6650 (2020).
35. M. E. Doroshenko, H. Jelínková, M. Jelínek, A. Říha, J. Šulc, N. O. Kovalenko, and I. S. Terzin, "Comparison of novel Fe^{2+}:$Zn_{1-x}Mn_xTe$ ($x \approx 0.3$) laser crystal operating near 5 µm at 78 K with other known Mn co-doped A^{II}-B^{VI} solid solutions," Opt. Mater. **108**, 110392 (2020).
36. M. E. Doroshenko, H. Jelínková, V. V. Osiko, M. Jelínek, D. Vyhlídal, J. Šulc, M. Němec, N. O. Kovalenko, and A. S. Gerasimenko, "Fe:ZnMnSe laser active material at 78–300 K: Spectroscopic properties and laser generation at 4.2–5.0 µm," J. Lumin. **192**, 1300–1307 (2017).
37. M. E. Doroshenko, V. V. Osiko, H. Jelínková, M. Jelínek, J. Šulc, M. Němec, D. Vyhlídal, M. Čech, N. O. Kovalenko, and A. S. Gerasimenko, "Spectroscopic and laser properties of bulk iron doped zinc magnesium selenide Fe:ZnMgSe generating at 4.5–5.1 µm," Opt. Express **24**(17), 19824–19834 (2016).

Optics EXPRESS

38. M. E. Doroshenko, H. Jelínková, M. Jelínek, J. Šulc, D. Vyhlídal, N. O. Kovalenko, and I. S. Terzin, "Room temperature Fe^{2+}:$Cd_{1-x}Mn_xTe$ laser generating at 5.4–6 µm," Opt. Lett. **43**(20), 5058–5061 (2018).
39. H. Uehara, T. Tsunai, B. Y. Han, K. Goya, R. Yasuhara, F. Potemkin, J. Kawanaka, and S. Tokita, "40 kHz, 20 ns acousto-optically Q-switched 4 µm Fe:ZnSe laser pumped by a fluoride fiber laser," Opt. Lett. **45**(10), 2788–2791 (2020).
40. A. V. Pushkin, E. A. Migal, S. Tokita, Y. V. Korostelin, and F. V. Potemkin, "Femtosecond graphene mode-locked Fe:ZnSe laser at 4.4 µm," Opt. Lett. **45**(3), 738–741 (2020).
41. I. M. S. Vasilyev, M. Mirov, V. Smolski, D. Martyshkin, V. Fedorov, S. Mirov, and V. Gapontsev, "Progress in Cr and Fe doped ZnS/Se mid-IR CW and femtosecond lasers," Proc. SPIE **10193**, 101930U (2017).
42. A. V. Pushkin, E. A. Migal, H. Uehara, K. Goya, S. Tokita, M. P. Frolov, Y. V. Korostelin, V. I. Kozlovsky, Y. K. Skasyrsky, and F. V. Potemkin, "Compact, highly efficient, 2.1-W continuous-wave mid-infrared Fe:ZnSe coherent source, pumped by an Er:ZBLAN fiber laser," Opt. Lett. **43**(24), 5941–5944 (2018).
43. S. Mirov, V. Fedorov, D. Martyshkin, I. Moskalev, M. Mirov, and S. Vasilyev, "High Average Power Fe:ZnSe and Cr:ZnSe Mid-IR Solid State Lasers," in *Advanced Solid State Lasers, 2015 OSA Technical Digest (online)* (Optical Society of America, 2015), paper AW4A.1.
44. V. I. Kozlovsky, Y. V. Korostelin, Y. P. Podmar'kov, Y. K. Skasyrsky, and M. P. Frolov, "Middle infrared Fe^{2+}:ZnS, Fe^{2+}:ZnSe and Cr^{2+}:CdSe lasers: new results," J. Phys.: Conf. Ser. **740**, 012006 (2016).
45. N. Myoung, V. V. Fedorov, S. B. Mirov, and L. E. Wenger, "Temperature and concentration quenching of mid-IR photoluminescence in iron doped ZnSe and ZnS laser crystals," J. Lumin. **132**(3), 600–606 (2012).
46. Y. O. Aydin, V. Fortin, R. Vallee, and M. Bernier, "Towards power scaling of 2.8 µm fiber lasers," Opt. Lett. **43**(18), 4542–4545 (2018).
47. W. Zhou, D. Wu, Q.-Y. Lu, S. Slivken, and M. Razeghi, "Single-mode, high-power, mid-infrared, quantum cascade laser phased arrays," Sci. Rep. **8**(1), 14866 (2018).
48. M. V. Chukichev, V. P. Chegnov, R. R. Rezvanov, O. I. Chegnova, V. P. Kalinushkin, and A. A. Gladilin, "Mid-IR Cathodoluminescence of Fe:ZnSe," Opt. Spectrosc. **125**(6), 870–873 (2018).
49. S. D. Velikanov, E. M. Gavrishchuk, N. A. Zaretsky, A. V. Zakhryapa, V. B. Ikonnikov, S. Y. Kazantsev, I. G. Kononov, A. A. Maneshkin, D. A. Mashkovskii, E. V. Saltykov, K. N. Firsov, R. S. Chuvatkin, and I. M. Yutkin, "Repetitively pulsed Fe:ZnSe laser with an average output power of 20 W at room temperature of the polycrystalline active element," Quantum Electron. **47**(4), 303–307 (2017).
50. V. A. Akimov, M. P. Frolov, Y. V. Korostelin, V. I. Kozlovsky, A. I. Landman, Y. P. Podmar'kov, and A. A. Voronov, "Vapour growth of II-VI single crystals doped by transition metals for mid-infrared lasers," Phys. Status Solidi C **3**(4), 1213–1216 (2006).
51. V. J. Hare, E. Loftus, A. Jeffrey, and C. B. Ramsey, "Atmospheric CO_2 effect on stable carbon isotope composition of terrestrial fossil archives," Nat. Commun. **9**(1), 252 (2018).
52. J. P. Ferrio, M. Aguilera, J. Voltas, and J. L. Araus, "Chapter Three - Stable carbon isotopes in archaeological plant remains," in *Stratigraphy & Timescales*, M. Montenari, ed. (Academic Press, 2020).
53. S. Guillon, E. Pili, and P. Agrinier, "Using a laser-based CO_2 carbon isotope analyser to investigate gas transfer in geological media," Appl. Phys. B **107**(2), 449–457 (2012).
54. T. Zhou, T. Wu, Q. Wu, C. Ye, R. Hu, W. Chen, and X. He, "Real-time measurement of CO2 isotopologue ratios in exhaled breath by a hollow waveguide based mid-infrared gas sensor," Opt. Express **28**(8), 10970–10980 (2020).
55. T. B. Sauke and J. F. Becker, "Stable isotope laser spectrometer for exploration of Mars," Planet. Space Sci. **46**(6-7), 805–812 (1998).
56. T. P. Belikova, E. A. Sviridenkov, and A. F. Suchkov, "Investigation of weak absorption and gain lines of some gases by the method of selective losses in a laser resonator," Quantum Electron. **4**(4), 454–456 (1974).
57. B. Henderson, A. Khodabakhsh, M. Metsälä, I. Ventrillard, F. M. Schmidt, D. Romanini, G. A. D. Ritchie, S. te Lintel Hekkert, R. Briot, T. Risby, N. Marczin, F. J. M. Harren, and S. M. Cristescu, "Laser spectroscopy for breath analysis: towards clinical implementation," Appl. Phys. B **124**(8), 161 (2018).
58. R. Ghorbani and F. M. Schmidt, "Real-time breath gas analysis of CO and CO_2 using an EC-QCL," Appl. Phys. B **123**(5), 144 (2017).
59. J. M. Eiler, ""Clumped-isotope" geochemistry—The study of naturally-occurring, multiply-substituted isotopologues," Earth Planet. Sci. Lett. **262**(3-4), 309–327 (2007).
60. I. Prokhorov, T. Kluge, and C. Janssen, "Laser Absorption Spectroscopy of Rare and Doubly Substituted Carbon Dioxide Isotopologues," Anal. Chem. **91**(24), 15491–15499 (2019).
61. V. M. Baev, G. Gaida, H. Schröder, and P. E. Toschek, "Quantum fluctuations of a multi-mode laser oscillator," Opt. Commun. **38**(4), 309–313 (1981).
62. M. P. Frolov, Y. V. Korostelin, V. I. Kozlovsky, and Y. K. Skasyrsky, "Study of a room temperature, monocrystalline Fe:ZnSe laser, pumped by a high-energy, free-running Er:YAG laser," Laser Phys. **29**(8), 085004 (2019).
63. T. J. Griffis, Z. Chen, J. M. Baker, J. D. Wood, D. B. Millet, X. Lee, R. T. Venterea, and P. A. Turner, "Nitrous oxide emissions are enhanced in a warmer and wetter world," Proc. Natl. Acad. Sci. U. S. A. **114**(45), 12081–12085 (2017).
64. K. Kantnerová, L. Yu, D. Zindel, M. S. Zahniser, D. D. Nelson, B. Tuzson, M. Nakagawa, S. Toyoda, N. Yoshida, L. Emmenegger, S. M. Bernasconi, and J. Mohn, "First investigation and absolute calibration of clumped isotopes in N_2O by mid-infrared laser spectroscopy," Rapid Commun. Mass Spectrom. **34**(15), e8836 (2020).

Optics EXPRESS

65. M. Yamaya, K. Sekizawa, S. Ishizuka, M. Monma, K. Mizuta, and H. Sasaki, "Increased Carbon Monoxide in Exhaled Air of Subjects with Upper Respiratory Tract Infections," Am. J. Respir. Crit. Care Med. **158**(1), 311–314 (1998).
66. K. Zayasu, K. Sekizawa, S. Okinaga, M. Yamaya, T. Ohrui, and H. Sasaki, "Increased Carbon Monoxide in Exhaled Air of Asthmatic Patients," Am. J. Respir. Crit. Care Med. **156**(4), 1140–1143 (1997).
67. S. E. Deveci, F. Deveci, Y. Açik, and A. T. Ozan, "The measurement of exhaled carbon monoxide in healthy smokers and non-smokers," Br. J. Dis. Chest **98**(6), 551–556 (2004).
68. R. Ghorbani and F. M. Schmidt, "ICL-based TDLAS sensor for real-time breath gas analysis of carbon monoxide isotopes," Opt. Express **25**(11), 12743–12752 (2017).

DOI: 10.1364/OE.422926
URN: urn:nbn:de:hbz:464-20210604-102219-4